

The multicomponent synergistic effect of hierarchical $\text{Li}_{0.485}\text{La}_{0.505}\text{TiO}_3$ solid-state electrolyte for dendrite-free lithium-metal batteries

Huanhui Chen, Liang Yu, Xing Cao, Qixin Yang, Ya Liu, Yanru Wei, Junrong Zeng, Liubiao Zhong, Yejun

Qiu*

Shenzhen Engineering Lab of Flexible Transparent Conductive Films, School of Materials Science and Engineering, Harbin Institute of Technology,

Shenzhen 518055, China

*Corresponding author.

Yejun Qiu, Email: yejunqiu@hit.edu.cn

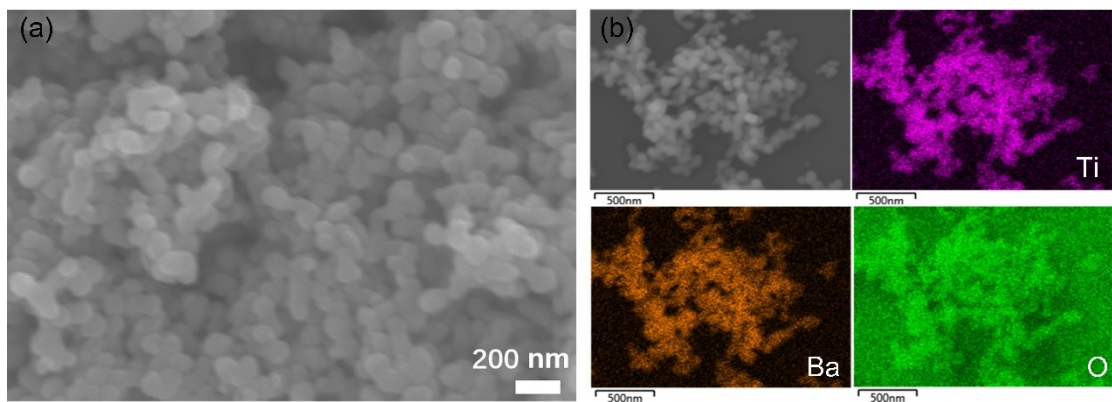


Fig. S1 (a) The SEM images of BTO and (b) SEM mapping of the BTO.

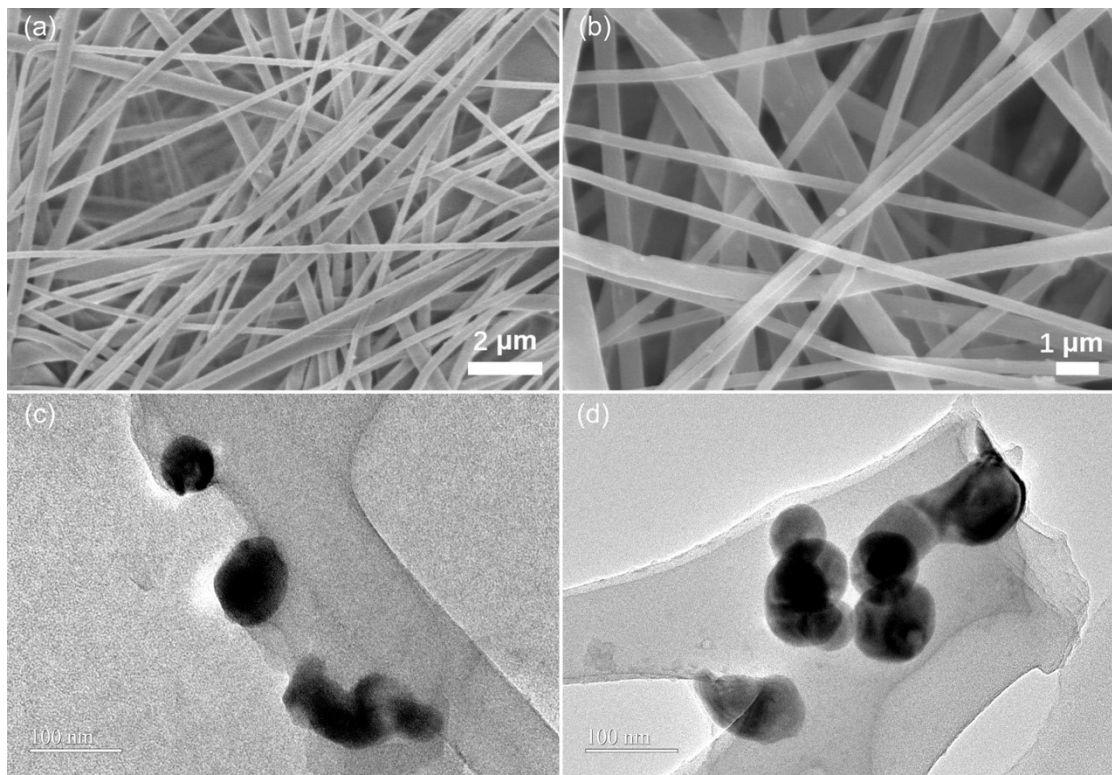


Fig. S2 (a-b) SEM images of BP; (c-d) TEM images of BP.

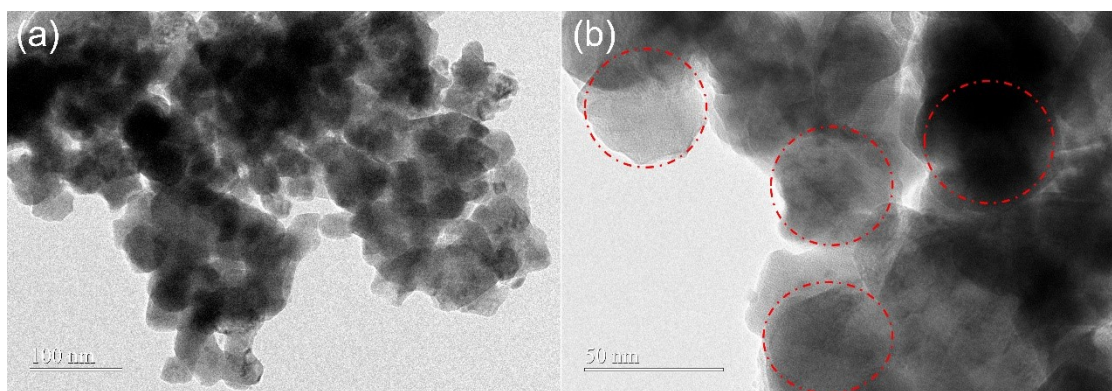


Fig. S3 The TEM images of the LLTO.



Fig. S4 (a) The digital photograph of the BP, (b) the thickness of BP film; (c) the digital photograph of the BP@LPFL, (d) the thickness of BP@LPFL membrane.

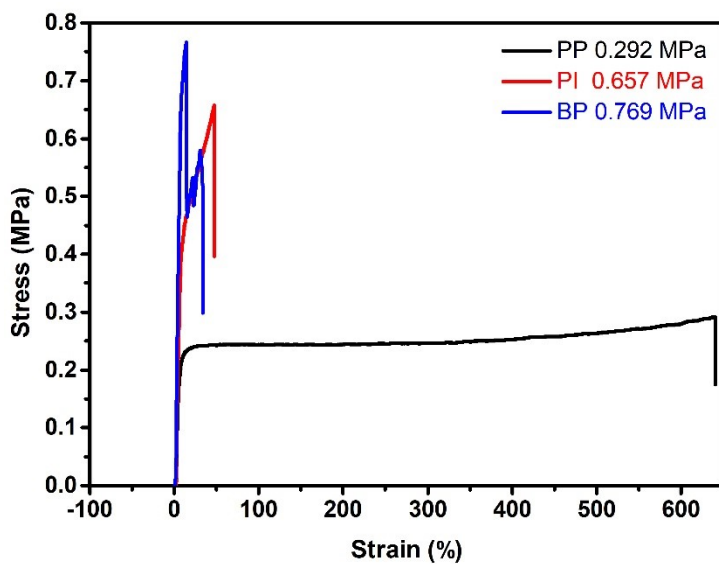


Fig. S5 The stress-strain behavior of the membrane.

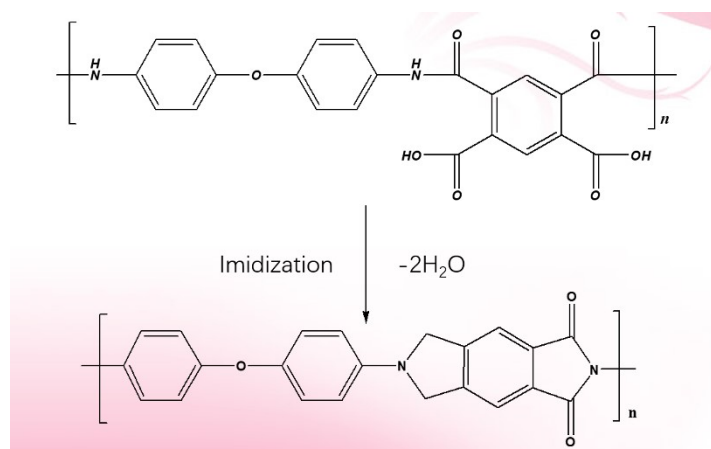


Fig. S6 The imidization reaction process.

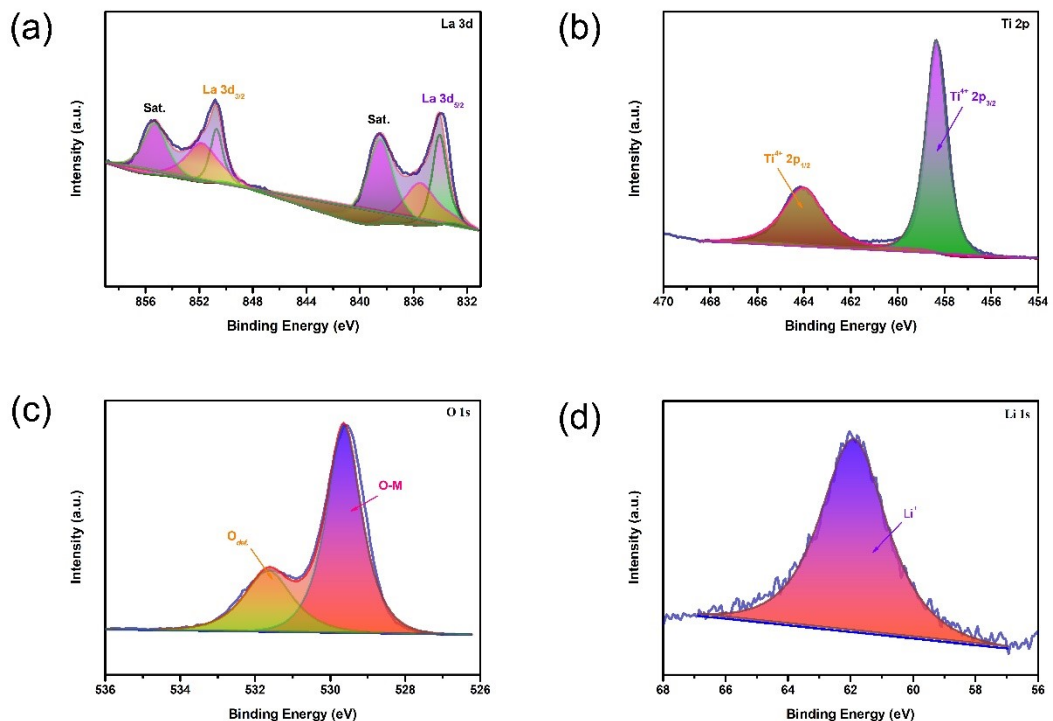


Fig. S7 Core level XPS spectra of LLTO electrolyte (a) La 3d, (b) Ti 2p, (c) O 1s and (d) Li 1s.

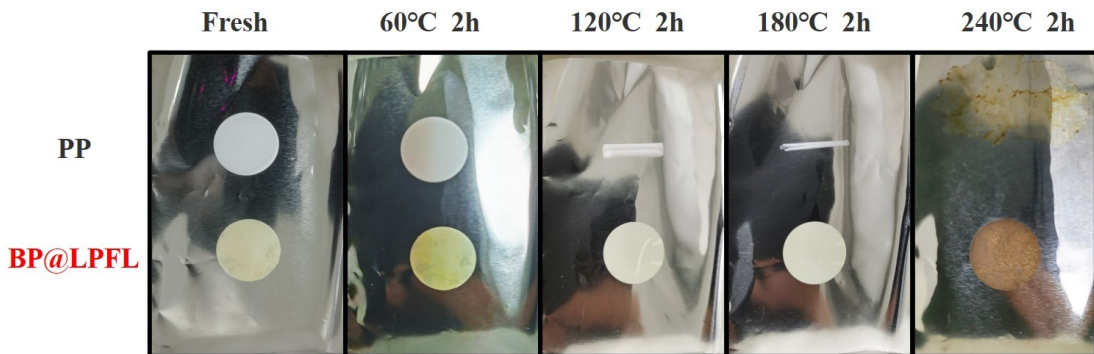


Fig.S8 Compared the thermal stability of BP@LPFL and conventional PP separator.

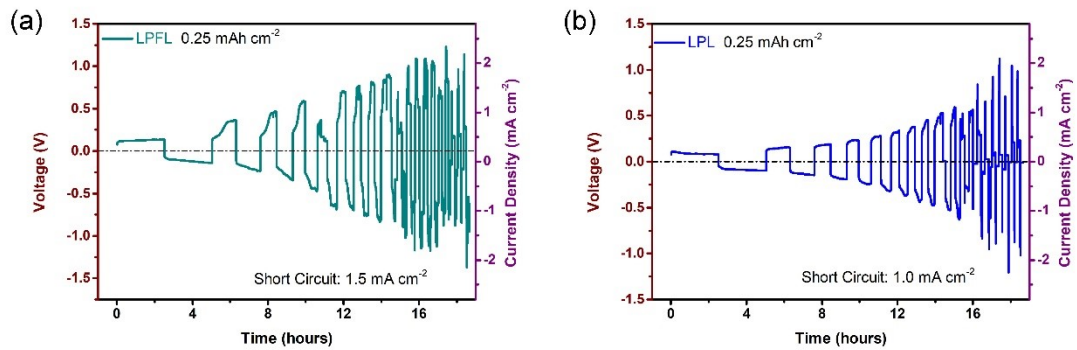


Fig. S9 The critical current density of Li-LPFL-Li cell (a) and Li-LPL-Li cell (b).

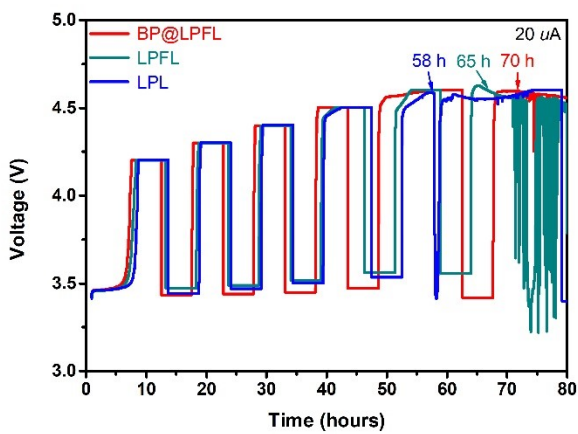


Fig. S10 The electrochemical floating analysis of BP@LPFL, LPFL and LPL using Li-LFP cell at 60 °C.

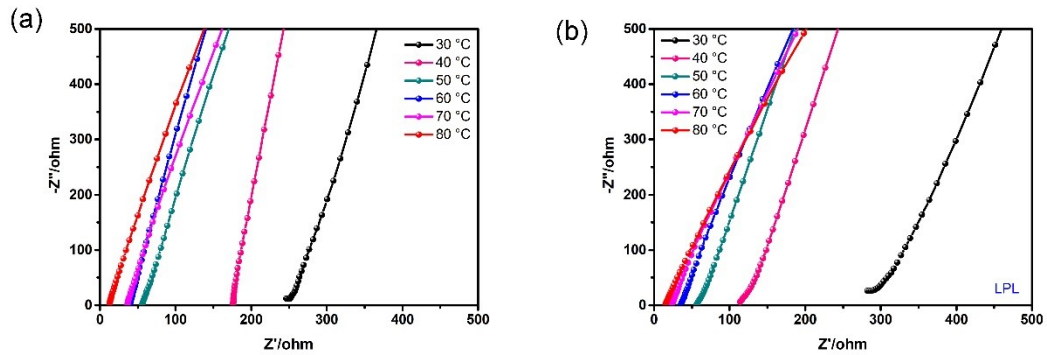


Fig. S11 (a) Nyquist plots of LPFL electrolyte at different temperature, (a) Nyquist plots of LPL electrolyte at different temperature.

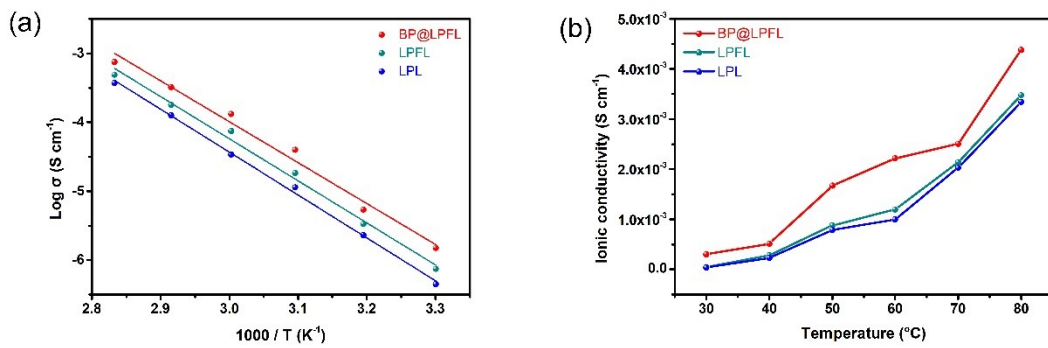


Fig. S12 (a) Arrhenius plots at different temperatures and (b) ionic conductivity curves.

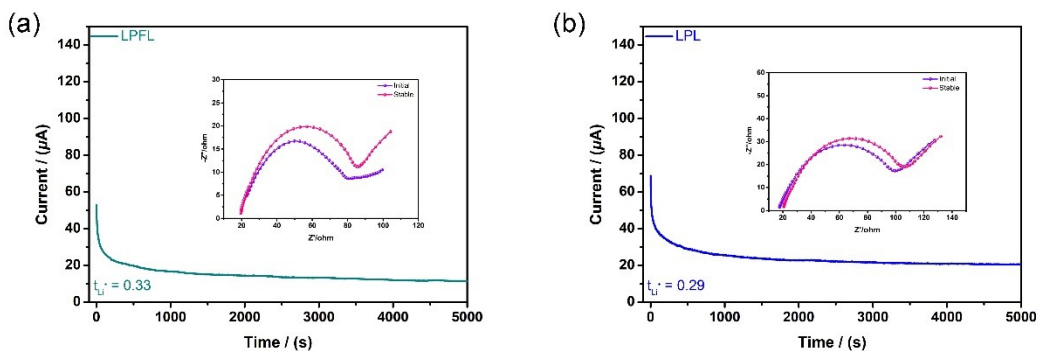


Fig. S13 Polarization curve and impedance diagram of the (a) LPFL and (b) LPL.

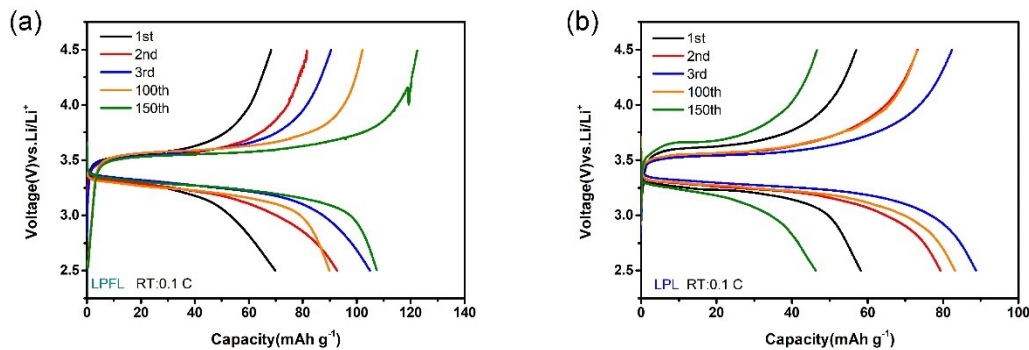


Fig. S14 (a) Discharge–charge curves of the Li-LPFL-LFP cell at 0.1 C and RT, (b) discharge–charge curves of the Li-LPL-LFP cell at 0.1 C

and RT.

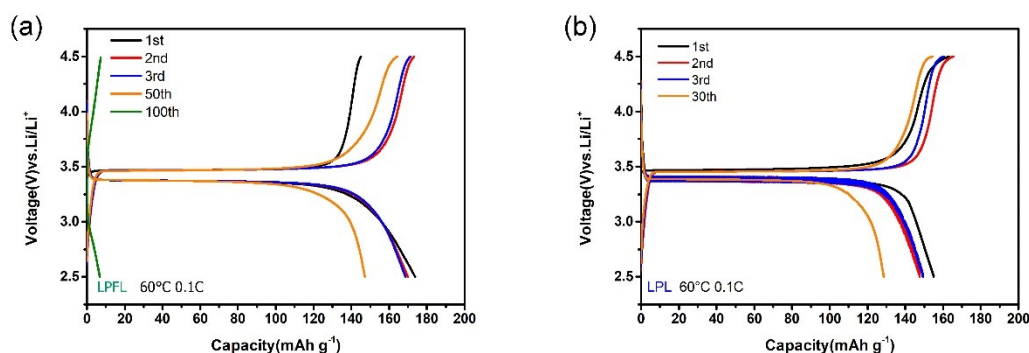


Fig. S15 (a) Discharge–charge curves of the Li-LPFL-LFP cell at 0.1 C and 60 °C, (b) discharge–charge curves of the Li-LPL-LFP cell at 0.1 C

and 60 °C.

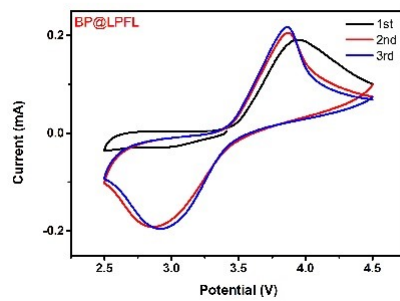


Fig. S16 CV curves of the Li-BP@LPFL-LFP cell at 0.2 mV s^{-1} .

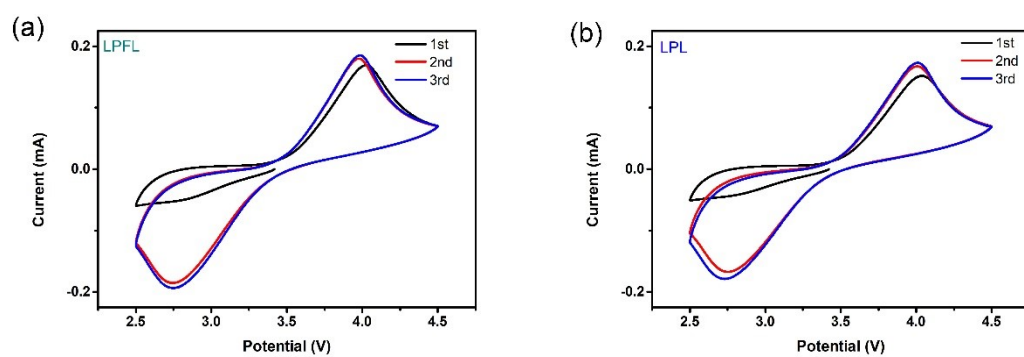


Fig. S17 (a) CV curves of the Li-LPFL-LFP cell at 0.2 mV s^{-1} and (b) CV curves of the Li-LPFL-LFP cell at 0.2 mV s^{-1} .

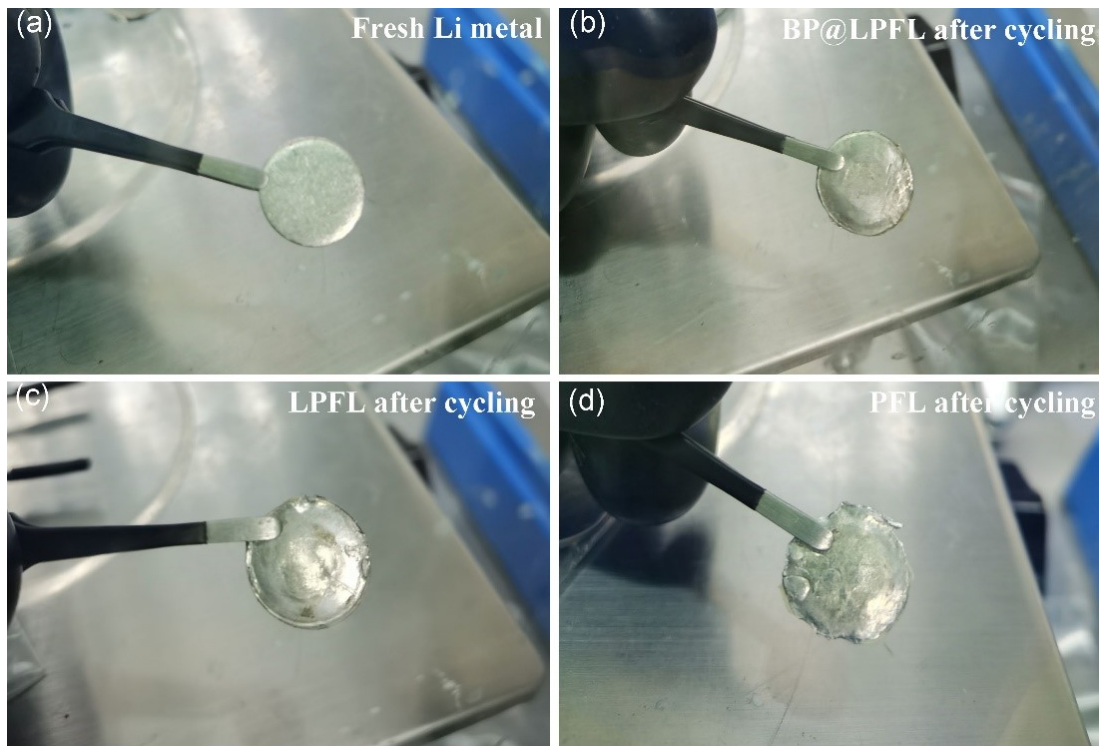


Fig. S18 The digital photograph of Li metal (a) fresh, (b) BP@LPFL after cycling, (c) LPFL after cycling, (d) LPL after cycling.

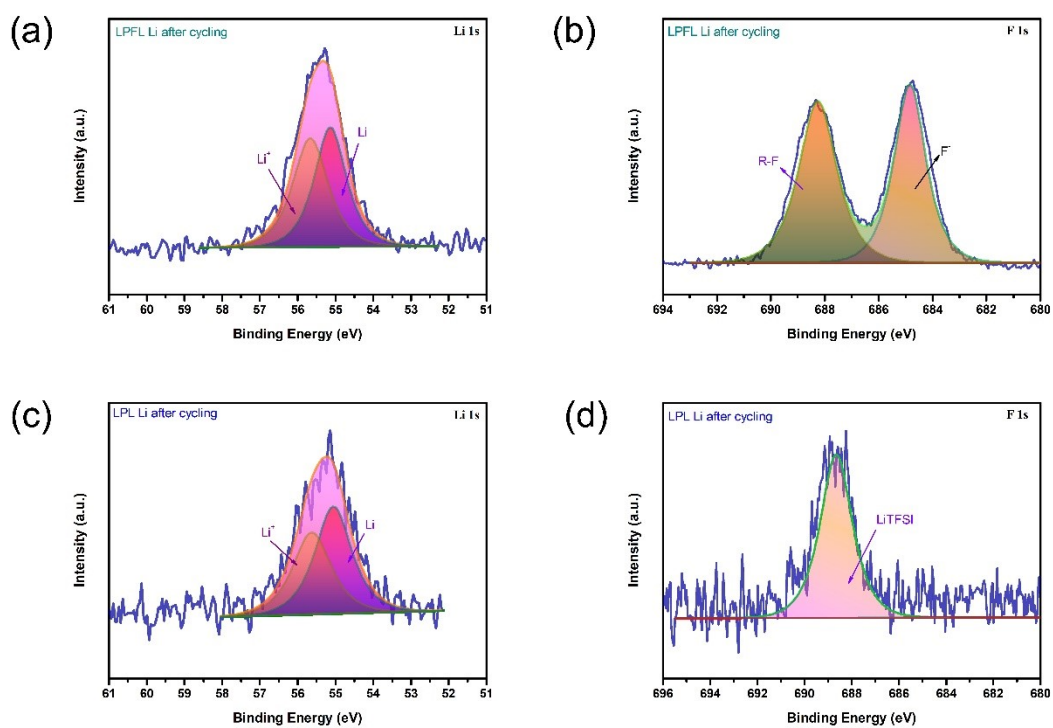


Fig. S19 XPS spectra of Li 1s (a) and F1s (b) for Li metal in Li-LPFL-LFP cell after cycling; XPS spectra of Li 1s (c) and F1s (d) for Li metal in

Li-LPL-LFP cell after cycling.

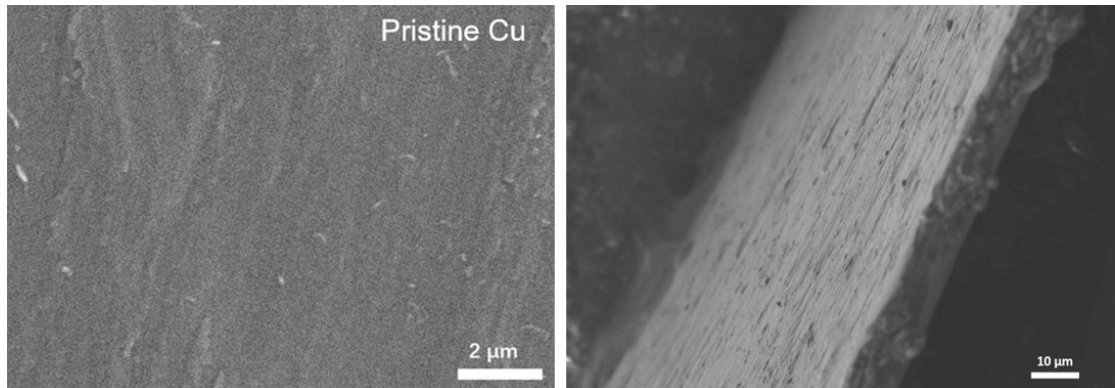


Fig. S20 The SEM and cross-sectional images of Cu foil.

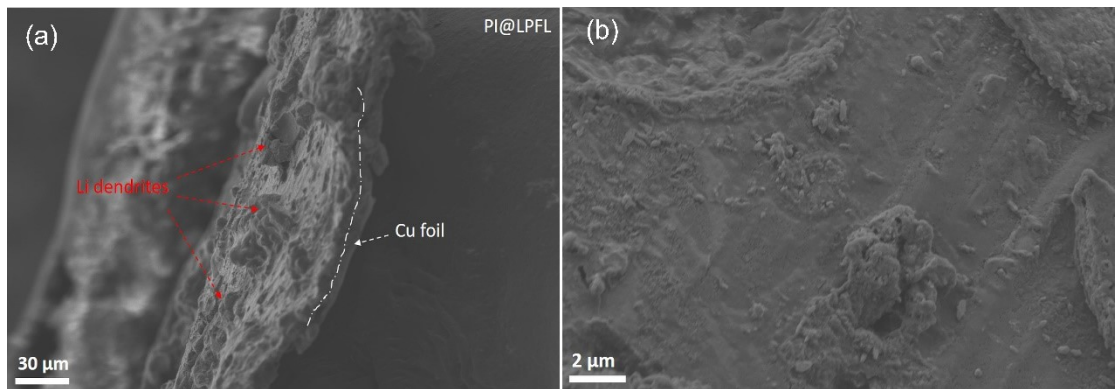


Fig. S21 The SEM images of Li deposition on Cu foil through PI@LPFL film.

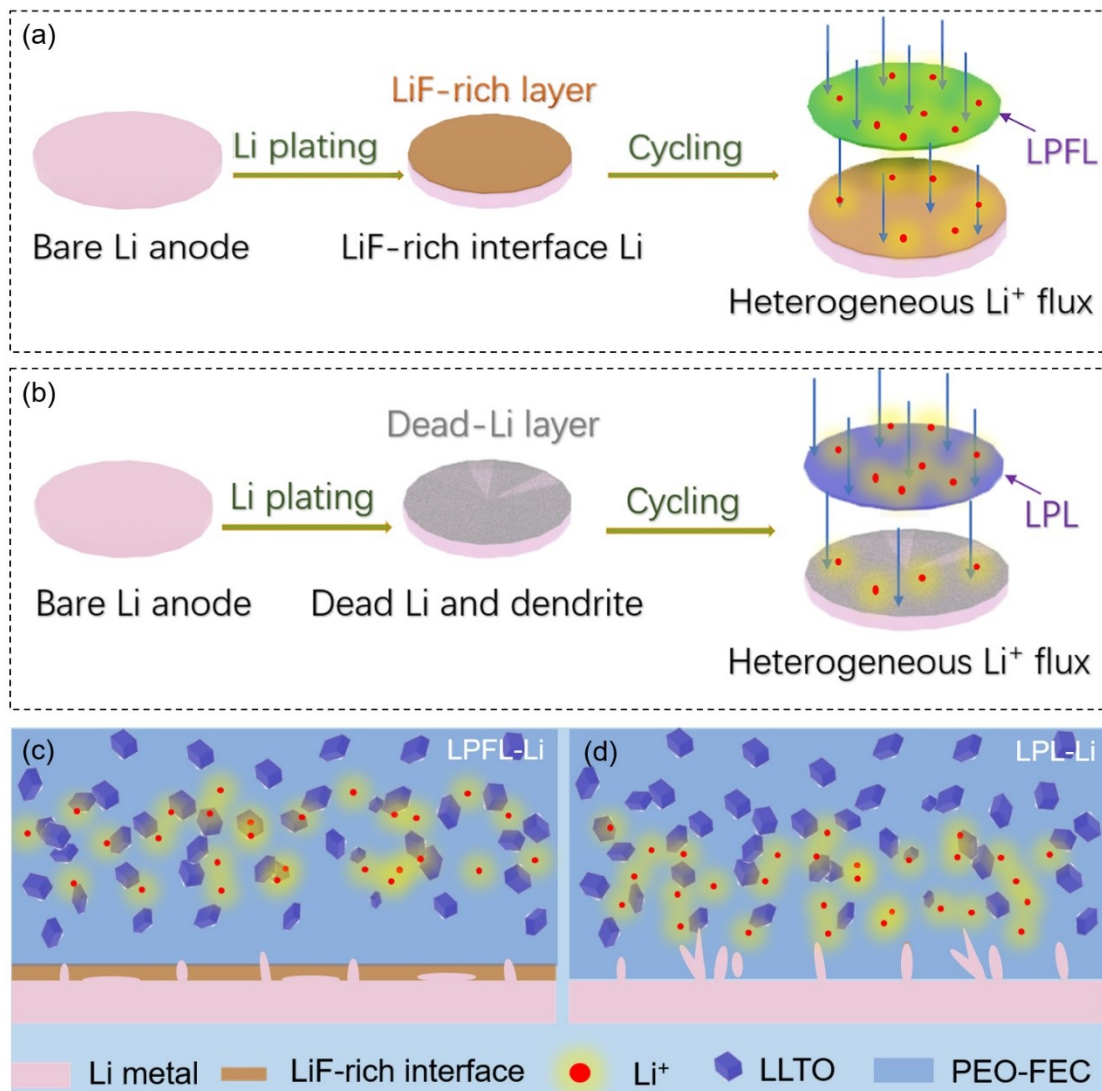


Fig. S22 Schematic illustration of the lithium deposition mechanism on Li metal (a) Li/LPFL/LFP and (b) Li/LPL/LFP; the evolution of Li plating/stripping on Li metal (c) Li/LPFL/LFP and (d) Li/LPL/LFP.

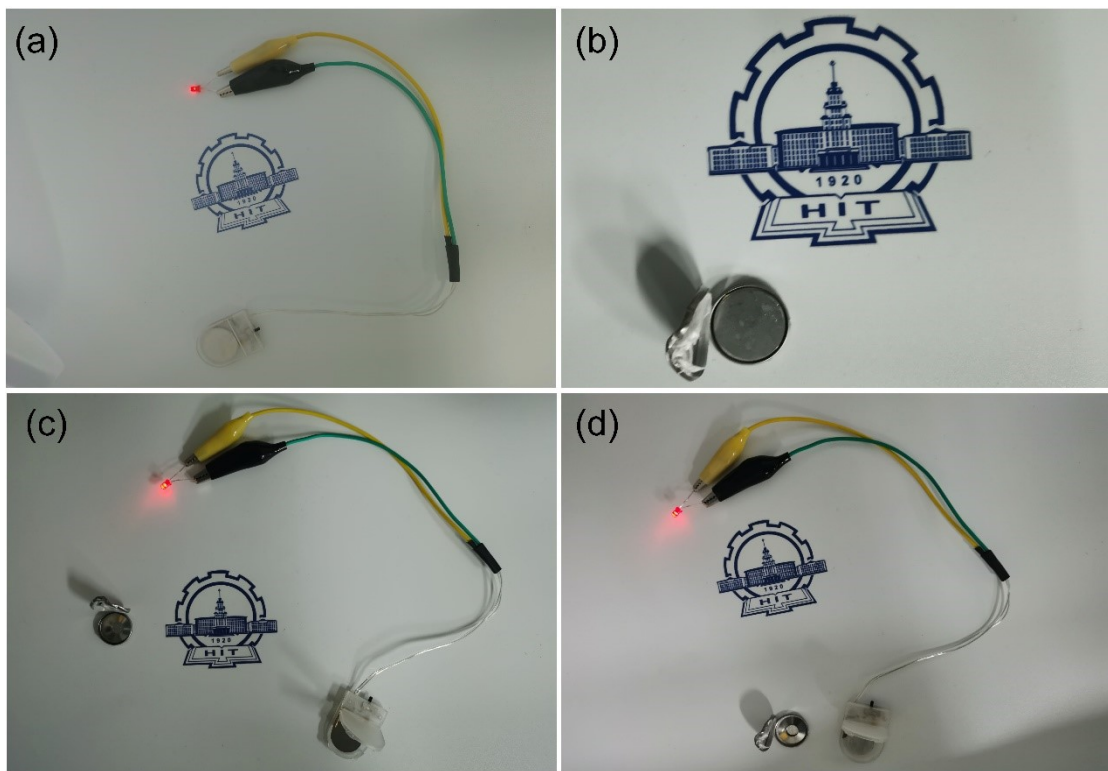


Fig. S23 (a) Digital photograph of the Li/BP@LPFL/LFP coin cell to turn on an LED lamp, (b) The Li/BP@LPFL/LFP coin cell after removing

stainless steel shell, (c) and (d) a LED lit up by battery under removing stainless steel shell.

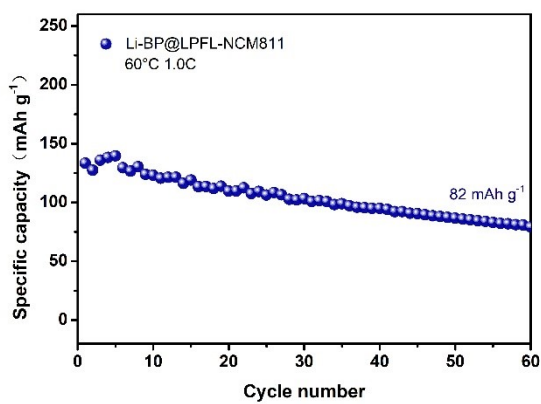


Fig. S24 The cycling performance of the Li/BP@LPFL/NCM811 battery at 1.0 C.

Table S1. Comparison of the performance of the BP@LPFL composite electrolyte with the literature data.

Materials	Performance				Ref.
	Current density	Current density 0.1C/60°C	Current density	Ionic conductivity S cm⁻¹/ RT	
	0.1 C/RT	1C/60°C			
LLTO film		125/50th (65°C)		2.0×10^{-5}	¹
PVD-FHFP/LiTFSI /LLATO/Li ₃ PO ₄	115/160th (0.5 C)			5.1×10^{-4}	²
LLTO-PEO-FEC	115/100th			1.1×10^{-4}	³
LLTOOnws-PAN-LiClO ₄				6.0×10^{-5}	⁴
PAN-LiClO ₄ -LLTO				2.4×10^{-4}	⁵
PVDF-b-PTFE-LLTO	127/550th (0.5 C)			1.4×10^{-4}	⁶
PEO-LLZTO	100/200th			1.6×10^{-4}	⁷
PAN/LLZTO/PEO	122/300th (0.2 C)	52/1700 th (RT)		1.76×10^{-4}	⁸
PI/PEO/LiTFSI		100/300th (0.5 C)		2.3×10^{-4}	⁹
PA/PEO/LiTFSI	100/100th	102/300th		2.0×10^{-4}	¹⁰
BP@LPFL	124/200th	165/110th	86/1000th	3.0×10^{-4}	This work

References

1. Z. Jiang, S. Wang, X. Chen, W. Yang, X. Yao, X. Hu, Q. Han and H. Wang, *Advanced Materials*, 2020, **32**, e1906221.
2. H. Yang, J. Bright, B. Chen, P. Zheng, X. Gao, B. Liu, S. Kasani, X. Zhang and N. Wu, *Journal of Materials Chemistry A*, 2020, **8**, 7261-7272.
3. H. Li, W. Liu, X. Yang, J. Xiao, Y. Li, L. Sun, X. Ren, P. Zhang and H. Mi, *Chemical Engineering Journal*, 2021, **408**, 127254.
4. W. Liu, S. W. Lee, D. Lin, F. Shi, S. Wang, A. D. Sendek and Y. Cui, *Nature Energy*, 2017, **2**.
5. W. Liu, N. Liu, J. Sun, P. C. Hsu, Y. Li, H. W. Lee and Y. Cui, *Nano Letters*, 2015, **15**, 2740-2745.
6. S. Liu, Y. Zhao, X. Li, J. Yu, J. Yan and B. Ding, *Advanced Materials*, 2021, **33**, e2008084.
7. H. Huo, Y. Chen, J. Luo, X. Yang, X. Guo and X. Sun, *Advanced Energy Materials*, 2019, **9**, 1804004.
8. Z. Zhang, YingHuang, G. Zhang and L. Chao, *Energy Storage Materials*, 2021, **41**, 631-641.
9. J. Wan, J. Xie, X. Kong, Z. Liu, K. Liu, F. Shi, A. Pei, H. Chen, W. Chen, J. Chen, X. Zhang, L. Zong, J. Wang, L. Q. Chen, J. Qin and Y. Cui, *Nature Nanotechnology*, 2019, **14**, 705-711.
10. Y. Xu, S. Zhang, T. Liang, Z. Yao, X. Wang, C. Gu, X. Xia and J. Tu, *ACS Applied Materials & Interfaces*, 2021, **13**, 11018-11025.